THE JOURNAL OF PHYSICAL CHEMISTRY C

Article

pubs.acs.org/JPCC

Density Functional Investigation of the Adsorption of Isooctane, Ethanol, and Acetic Acid on a Water-Covered Fe(100) Surface

Pedro O. Bedolla,*[,†,‡] Gregor Feldbauer,[†,‡] Michael Wolloch,[†,‡] Christoph Gruber,[†] Stefan J. Eder,[‡] Nicole Dörr,[‡] Peter Mohn,[†] Josef Redinger,[†] and András Vernes[†,‡]

[†]Institute of Applied Physics, Vienna University of Technology, Wiedner Hauptstrasse 8-10/134, 1040 Vienna, Austria

[‡]Austrian Center of Competence for Tribology, Viktor-Kaplan-Strasse 2, 2700 Wiener Neustadt, Austria

Supporting Information

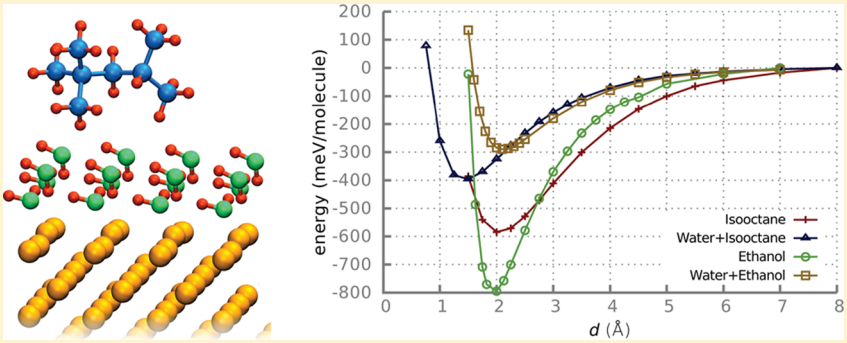

ABSTRACT: The presence of water in biofuels poses the question of how it affects the frictional performance of additives in fuels containing organic substances. To investigate the effect of water on the adsorption of molecules present in fuel and its additives we simulated within the framework of density functional theory the adsorption of ethanol, isooctane (2,2,4-trimethylpentane), and acetic acid on a bare and a water-covered Fe(100) surface. Van der Waals interactions are taken into account in our computations. In those molecules, where dispersion forces contribute significantly to the binding mechanism, the water layer has a stronger screening effect. Additionally, this effect can be enhanced by the presence of polar functional groups in the molecule. Thus, with the introduction of a water layer, the adsorption energy of isooctane and ethanol is reduced but it is increased in the case of the acetic acid. The adsorption configuration of ethanol is changed, while the one of acetic acid is moderately, and for isooctane only very slightly altered. Therefore, the effect of a water layer in the adsorption of organic molecules on an Fe(100) surface strongly depends on the type of bond and consequently, so do the tribological properties.

INTRODUCTION

With a production surpassing 100 billion liters per year, biofuels have become an important part of the motor fuel consumption in the world, where ethanol continues to be the most common biofuel worldwide.[1] Because of its high energy density, ethanol has also been considered one of the most important renewable resources for the production of hydrogen for transportation and stationary power fuel cell applications.[2−5] The steam reforming reaction[6] in which ethanol reacts with water ($C_2H_5OH + 3H_2O \rightarrow 2CO_2 + 6H_2$) has been the subject of study during the past decade as a promising mechanism to produce hydrogen.[7−10] Although these studies have focused on the search for catalysts that minimize the formation of undesirable intermediates and maximize the conversion of ethanol, the presence of water in biofuels also poses the question of how the effectiveness of additives in fuels containing organic substances is affected.

A crucial step toward an answer is to improve our understanding of the interaction between the organic molecules (the fuel and the additive), water, and metallic surfaces (the fuel pump, the combustion chamber, etc.). For this purpose, various theoretical approaches, such as density functional theory (DFT),[11] have proven to be useful as they have been able to calculate adsorption energies as well as configurations of various combinations of organic molecules on metallic surfaces.[12] During the past decade, several functionals have been developed to take van der Waals (vdW) forces into account[13−42] and additional studies have shown that it is necessary to use DFT functionals that include nonlocal correlation in order to describe the adsorption process correctly.[43−52] Only a few theoretical studies have analyzed the effects of water on the adsorption of organic molecules, including a rigorous treatment of the van der Waals interactions. On an ab initio level, the effects of a water layer on the adsorption of methanol and formaldehyde on Pt(111) was studied by Błonski and López,[53] and more recently, a density functional investigation of the adsorption of a water−ethanol mixture on Pt(111) was carried out by Tereshchuk and Da Silva.[54] These studies considered a platinum surface because

Received: May 13, 2014
Revised: July 31, 2014
Published: September 9, 2014

   dx.doi.org/10.1021/jp504695m | J. Phys. Chem. C 2014, 118, 21428−21437

of its catalytic potential; however, in many industrial and technological applications where the lubrication additives in fuels play an important role, the involved metallic surface is often iron or some alloy derived from it. In gasolines, several types of organic compounds may be present, such as alcohols, organic acids, and branched alkanes. The interaction between iron and water is a complex chemical process that may lead to dissociation of the water molecule. However, earlier experiments and theoretical calculations suggest the presence of adsorbed molecular water at high water coverages.[55−59]

To investigate the effect of water on the adsorption of molecules present in fuels and its additives, we simulated the adsorption of isooctane (2,2,4-trimethylpentane), ethanol, and acetic acid [with chemical formulas $(CH_3)_3CCH_2CH(CH_3)_2$, CH_3CH_2OH, and CH_3COOH, respectively] on a water-covered Fe(100) surface via first-principles calculations. These adsorbates were selected because isooctane is a representative aliphatic gasoline compound, ethanol can be found in gasoline as a biocomponent as well as in many other relevant products, and acetic acid may be introduced into fuels as a possible trace contaminant of ethanol. Furthermore, the interaction between the acetic acid and the iron surface is representative of the one occurring between fatty acids, commonly found in fuels as lubricity additives, and metallic surfaces. These fatty acids have chain lengths of typically C_{14}−C_{18}. Therefore, the choice of acetic acid minimizes the effect of vdW forces between aliphatic chains and solely focuses on interactions with the surface. The various functional groups contained in the selected molecules facilitate the investigation of their distinct effects on the adsorption process. The Fe(100) surface, besides being present in systems of industrial interest, has been considered in various previous studies that investigate the adsorption of water on iron.[55−58,60,61] Therefore, the selection of this surface is advantageous for comparing and validating our results. A formal description of van der Waals interactions as implemented in the optB86b-vdW functional,[62] which is limited to pairwise interactions but it is otherwise independent of external input parameters, is applied. The approaches that go beyond the pairwise additivity and include the vdW energy very accurately, such as the random phase approximation[30,32−34] combined with the adiabatic connection and fluctuation dissipation theorem,[29,31] are computationally prohibitive for the systems treated in this work. This paper describes the changes in the adsorption energy and equilibrium geometries induced by a water layer and discusses these alterations on the basis of the electronic density.

COMPUTATIONAL DETAILS

To perform our simulations, we carried out spin-polarized first-principles calculations within the framework of density functional theory using the Vienna Ab Initio Simulation Package (VASP).[63−68] VASP produces an iterative solution of the Kohn−Sham equations using a plane-wave basis and employing periodic boundary conditions. The projector augmented wave (PAW) method[69] was applied to describe the interaction between the core and the valence electrons. The vdW interactions were taken into account via the optimized Becke86[70] van der Waals (optB86b-vdW) exchange−correlation functional,[62,71]

$$E_{xc}^{\text{optB86b-vdW}}[n] = E_{\text{optB86b(x)}}[n] + E_{\text{LDA(c)}}[n] + E_{\text{nl(c)}}[n] \quad (1)$$

where n is the electronic density in the ground state, $E_{\text{optB86b(x)}}[n]$ is a reparametrized version of the Becke86 exchange functional, $E_{\text{LDA(c)}}[n]$ is a local-density approximation (LDA) correlation, and $E_{\text{nl(c)}}[n]$ is a nonlocal correlation term that approximates the vdW interactions.

To model the adsorption of various molecules on an Fe(100) surface, we constructed a slab consisting of 10 layers of body-centered cubic (bcc) Fe and a corresponding molecule placed on one side of the slab at a distance d above it. In modeling the adsorption of water molecules, (1×1), (2×1), and (2×2) surface cells were studied, placing one, two, and four water molecules, respectively. This allows for more flexibility in determining the water layer structure by analyzing various possible scenarios, such as those where all the water molecules are constrained to the same geometry [(1×1) cell] and either two [(2×1) cell] or four [(2×2) cell] different orientations of the water molecules are allowed. In the adsorption of organic molecules a (4×4) surface cell was considered. The vacuum spacing in the z-direction between repeated iron slabs was 29.73 Å. The z axis is perpendicular to the metallic surface and starts at the bottom layer of the iron slab. This setup accurately models a bcc Fe(100) surface, avoids slab−slab interactions, and, in the cases were a single molecule was adsorbed, also avoids intermolecular interactions. Dipole corrections were checked but found to be negligible for this setup. The lattice constant of 2.83 Å used to construct the iron slab was obtained from a bulk calculation for bcc iron using the PBE[72,73] functional, where the calculation parameters were chosen to keep the accuracy consistent with the rest of the computations. This value is in good agreement with the experimental lattice constant of 2.86 Å.[74] The distance d was defined as the vertical distance between the atom of the molecule with lowest z coordinate and the closest atom to it, whether it is an atom belonging to the water layer (if present) or to the iron surface. For the dissociated acetic acid, the distance d is measured between the acetate and the metallic surface.

To ensure sufficiently accurate total energies and forces, we carefully selected and tested our calculation parameters. A tight convergence criterion of 10^{-6} eV on the total energy in the self-consistency cycle was used and a cutoff energy of 400 eV was applied for the plane-wave basis set. For the calculations involving a (4×4) surface cell, the k-space integrations were performed using a $2 \times 2 \times 1$ Monkhorst−Pack mesh.[75,76] For the smaller cells used to model the adsorption of water molecules, a corresponding mesh that generates the same k-point density was applied. The tetrahedron method with Blöchl corrections was employed for the static calculations and a Gaussian smearing with a width of 0.2 eV for the relaxations. Test calculations with smaller widths were carried out to ensure that the selected value leads to the ground-state geometry. The conjugate gradient algorithm was used to relax most of the structures, allowing the ions to move until an energy convergence criterion of 10^{-5} eV was fulfilled. For those cases where the starting guess was unreliable, a damped molecular dynamics algorithm was preferred. During relaxations, the ions in the top four layers of the slab and the ones constituting the molecule and the water layer (if present) were allowed to move in all directions, while the atoms in the six remaining layers of the slab were frozen at bulklike positions. Due to the complexity of the system, only the relaxations involving the water molecules and the iron slab were verified by performing a simulated annealing. The simulation started at a

dx.doi.org/10.1021/jp504695m | J. Phys. Chem. C 2014, 118, 21428−21437

temperature of 300 K and the temperature was gradually decreased to 0 K in 10 ps (10 000 time steps).

To produce an accurate description of the interaction between the organic molecules treated in this work and the iron surface, we calculated the potential energy curves by varying d and subsequently computing the total energy of the resulting system via static calculations. These curves will aid in the fitting of potentials required for classical molecular dynamic simulation, allowing the study of these systems in a different time and length scale. The equilibrium distance was considered to be the value of d that minimizes the total energy of the system. We stress that this equilibrium distance is obtained from a finite set of energy points calculated for various values of d, and therefore, its accuracy depends on the step size (Δd) between those values. To obtain a first estimate of the equilibrium structure, the potential energy curves of different configurations and adsorption sites were calculated with moderate values of Δd. The adsorption energies were calculated according to the equation

$$E_{ads} = E_{tot}^{mol+Fe(100)} - (E_{tot}^{mol} + E_{tot}^{Fe(100)}) \quad (2)$$

where $E_{tot}^{mol+Fe(100)}$ is the total energy of the products adsorbed on the Fe(100) slab at the equilibrium distance, $E_{tot}^{Fe(100)}$ is the total energy of the clean Fe(100) slab, and E_{tot}^{mol} is the total energy of the isolated gas-phase educts calculated using a cubic box with 15 Å side length. In the presence of a water layer,

$$E_{ads} = E_{tot}^{mol+H_2O+Fe(100)} - (E_{tot}^{mol} + E_{tot}^{H_2O+Fe(100)}) \quad (3)$$

was used instead. In this latter equation $E_{tot}^{H_2O+Fe(100)}$ is the total energy of the water-covered Fe(100) slab, $E_{tot}^{mol+H_2O+Fe(100)}$ is the total energy of the products adsorbed on the water-covered Fe(100) surface at the equilibrium distance, and E_{tot}^{mol} is the energy of the gas-phase educts as indicated above. Because of the magnitude of the step size, the adsorption energies and equilibrium distances obtained in this way are only an approximation, and thus, they will be referred to as such in the rest of this paper. The resulting most favorable configuration of this analysis was relaxed and used as an input to calculate a more accurate adsorption energy and equilibrium distance using a smaller value of Δd.

RESULTS AND DISCUSSION

Isooctane, Ethanol, and Acetic Acid on Bare Fe(100). In the equilibrium configuration, the isooctane molecule is oriented with its longest continuous chain of carbon atoms parallel to the Fe(100) surface (Figure 1a–c). A similar result was found in our previous investigation,[12] where the effects of vdW interactions on the adsorption of isooctane and ethanol on the same surface were analyzed. In the present study, however, the adsorption geometry plays a more important role, and therefore, we analyzed three orientations of the isooctane molecule (Figure 1a,c,d) in addition to the ones considered in ref 12. For comparison purposes, we included in our calculations the orientation of the isooctane molecule in the previously determined equilibrium configuration (Figure 1b). In each configuration, we studied the isooctane molecule adsorbed on the top, bridge, and hollow sites. The difference between the estimated adsorption energies of configurations 1–3 (≈ 0–70 meV) indicates that any of these may be reached at room temperature (≈ 25 meV) and that no particular adsorption site is preferred (see the Supporting Information). In contrast, the adsorption energies of configuration 4 are at least 162 meV lower than those calculated for the other configurations, although among them they did not show a preference for an adsorption site either. This is to be expected since, as we have shown,[12] the binding of the isooctane molecule to the metallic surface is dominated by dispersion forces, and thus, an orientation that maximizes the number of atoms in proximity to the surface is favored. We selected the adsorption configuration analyzed in our previous study, namely, configuration 2 with isooctane adsorbed on the top site, to carry out the rest of this study, because it is among the possible configurations existing at room temperature and also because we can apply our previous findings of the adsorption process. The lowest energy configuration (configuration 1) can also be employed for future investigations. In this configuration, the isooctane molecule is adsorbed at a distance $d \approx 2.25$ Å and orients its main C–C chain parallel to the metallic surface, as mentioned before. Its branches constituted by methyl groups are positioned away from the iron slab and above their parent chain (Figure 1a).

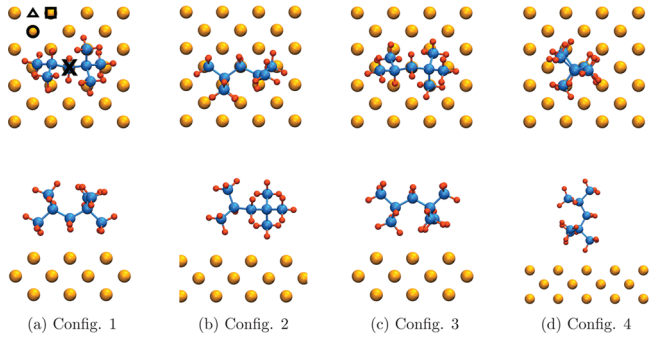

Figure 1. Configurations considered for the adsorption of an isooctane molecule on an Fe(100) surface, here displayed with the molecule on the top adsorption site at a distance d = 2.00 Å. The top row displays the top view of the system, while the bottom row shows the side view. The atom marked with an X symbol in the top view of configuration 1 is used as a reference to orient the molecule on the top, bridge, and hollow sites, indicated in the same figure with a circle, triangle, and square, respectively.

When ethanol is adsorbed on an Fe(100) surface, the hydroxyl group of the molecule orients parallel to the surface, while the remaining atoms of the molecule arrange accordingly (Figure 2a,c). Just as with isooctane, we extended our previous study[12] by considering three additional configurations of an

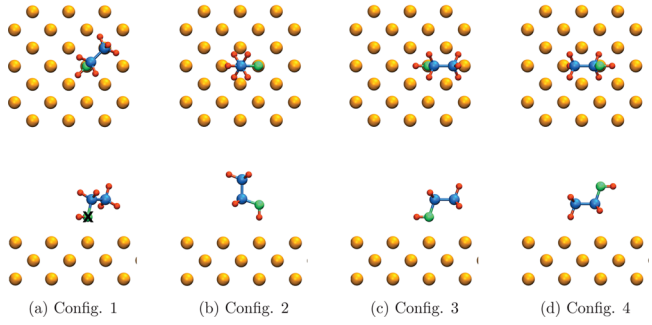

Figure 2. Configurations considered for the adsorption of an ethanol molecule on an Fe(100) surface, here presented analogously to Figure 1. The atom marked with an X symbol in the side view of configuration 1 (the oxygen atom of the hydroxyl group, colored in green) is used as a reference to orient the molecule in the adsorption sites.

dx.doi.org/10.1021/jp504695m | J. Phys. Chem. C 2014, 118, 21428–21437

ethanol molecule adsorbed on an Fe(100) surface (Figure 2a,b,d). As before, we included the orientation of the ethanol molecule found in ref 12 (Figure 2c) and we considered the molecule adsorbed on the top, hollow, and bridge sites in all configurations. In contrast to isooctane, the calculated adsorption energies are distributed among a larger energy range, and with the exception of configuration 4, there is notable energy difference between the adsorption sites (see the Supporting Information). The largest adsorption energy is achieved when the ethanol molecule is adsorbed on the top site and is oriented as in configuration 3, in agreement with our previous finding.[12] Our calculations show that this configuration is degenerate in energy with configuration 1 when the ethanol molecule is adsorbed on the top site. For the rest of the study, we considered configuration 2 in addition to these equilibrium structures, since a strong interaction between the hydroxyl group and the water molecules is expected.

If the carboxylic hydrogen of the acetic acid dissociates, the resulting acetate radical is adsorbed in a bidentate configuration. Experimental studies have suggested that the carboxylic hydrogen of the acetic acid molecule gets easily detached in the vicinity of clean metal, and metal oxide, surfaces.[70−80] For the dissociated molecule, these studies together with theoretical calculations for the adsorption on Ge(001)[81] and Fe(110)[82] surfaces have proposed monodentate and bidentate adsorption configurations. Moreover, in the latter study, no appreciable adsorption of the nondissociated acetic acid on an Fe(110) surface was found because dispersion forces were not included in the calculations. On the basis of these results, we considered the bidentate (Figure 3b) and the monodentate (Figure 3c)

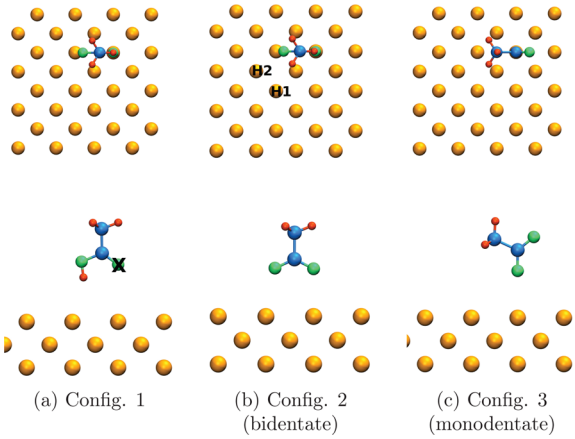

Figure 3. Configurations considered for the adsorption of acetic acid and acetate on an Fe(100) surface, here presented analogously to Figure 1. The atom with an X symbol in the side view of configuration 1 is used as a reference to orient the molecule on the adsorption sites. The two initial positions considered for the dissociated hydrogen are indicated as H1 (top) and H2 (hollow).

configurations for the adsorption of acetate, and since we are employing a vdW density functional for all computations, we also included the adsorption of the nondissociated acetic acid (Figure 3a). As was done with the previous compounds, the adsorption energies of the molecule adsorbed on the top, hollow, and bridge sites in each configuration were calculated. Depending on the nature of the carboxylic hydrogen dissociation, an acetate radical (homolytic cleavage) or an acetate anion (heterolytic cleavage) can be formed. A previous investigation on the adsorption of acetic acid on an Fe(110) surface[82] showed that, in the adsorbed state, the acetate radical is energetically favored over the anion. The results of our calculations show that this is also valid for the adsorption on the Fe(100) surface. The estimated adsorption energy of the acetic acid of 452 meV indicates that the molecule binds to the surface. This binding is nevertheless weak in comparison to those of the dissociated acetic acid species (Table 1). The

Table 1. Adsorption Energies and Equilibrium Distances of Various Molecules Adsorbed on a Bare and a Water-Covered Fe(100) Surface

	ads energy (eV)		eq dist (Å)	
molecule	no H_2O	with H_2O	no H_2O	with H_2O
isooctane	0.59	0.40	2.00	1.50
ethanol	0.80	0.29	2.00	2.10
acetic acid	2.48	3.18	1.95	1.25
acetate	4.49	5.18	2.00	1.50
acetate, H_2[a]	2.15		1.95	

[a]The calculated adsorption energy strongly depends on the source of H. See the text for further details.

highest adsorption energy is reached when the acetate radical is adsorbed in the bidentate configuration on the top site of the Fe(100) surface (see the Supporting Information), and thus, we selected this configuration to carry out further calculations.

Before introducing the water layer, a better approximation to the equilibrium structures and adsorption energies was obtained by relaxing the selected configuration of each system mentioned in this section. Each resulting structure was then used to calculate the potential energy curve by displacing the molecule in smaller steps. No large variations from the relaxed structure are expected at separations equal to or greater than the equilibrium distance. Indeed, further relaxations carried out for a few selected distances (d) to verify this assumption show variations on the order of 10^{-3} Å in bond lengths and 10^{-3} deg in angles. Since after the extended analysis no new configuration of isooctane and ethanol with a considerably higher adsorption energy was found, here we simply repeat the previously reported equilibrium distances and adsorption energies (Table 1) calculated in a previous study.[12] This facilitates the comparison of these values with those calculated in the presence of a water layer. After relaxing the acetate system, the oxygen atom on the top adsorption site is displaced by 0.08 Å toward the bridge site (moving the rest of the molecule accordingly) and the distance between the oxygen atoms is reduced by 0.03 Å. The iron atoms situated directly below the two oxygen atoms of the acetic acid are displaced 0.05 Å in the direction of the molecule. In equilibrium, the molecule is adsorbed on the slab at a distance of 2.00 Å, with an energy of 4.49 eV. At first sight, our results may suggest that the slab (and not the molecule) determines the equilibrium distance, since all the molecules are adsorbed at a distance of 2.00 Å. However, as mentioned before, these distances are an approximation that depends on the length of the step in d used for the static calculations. If the energy varied rapidly with d, we used a value of Δd = 0.125 Å; otherwise, we set Δd = 0.25 Å.

To study the dissociated acetic acid, additional systems were constructed. The adsorption of the acetate radical considered so far is useful for the construction of potentials that can be applied in classical molecular dynamics calculations, as stated before. This molecule fragment, however, does not exist under ordinary experimental conditions, and therefore, the hydrogen

dx.doi.org/10.1021/jp504695m | J. Phys. Chem. C 2014, 118, 21428−21437

atom cannot be neglected. In a recent study, where the adsorption of acetic acid on TiO_2 was analyzed,[83] it is indicated that there are three possible reaction paths for the dissociated hydrogen: formation of hydrogen gas, adsorption on the substrate, or reaction with a third substance. Other possible phenomena, such as the diffusion of hydrogen into the bulk (hydrogen embrittlement), are outside the scope of the present study, and thus, they are not discussed further. The formation of hydrogen gas was considered by introducing a H_2 molecule in the supercell shown in Figure 3b, followed by a relaxation of the ionic positions. In the equilibrium geometry, the hydrogen molecule is adsorbed on a top site with its molecular axis parallel to the surface. The adsorption of the dissociated hydrogen on the substrate was simulated by introducing a single hydrogen atom at the positions H1 and H2 marked on Figure 3b (one at a time) and relaxing the cell afterward. The hydrogen atom, initially in the H1 position, was displaced to a bridge site during the relaxation, while the one initially on the H2 position remained close to the hollow site, with a displacement of 0.4 Å away from the molecule. With an energy difference of 0.09 eV, the H atom on the bridge site is energetically more favorable than on the hollow site.

Depending on the availability of a second hydrogen atom, the dissociated hydrogen of the acetic acid may be adsorbed on the substrate or released as hydrogen gas. The comparison between the binding energies (Table 1) of these systems suggests that the adsorption of hydrogen on the substrate is favored over the formation of molecular hydrogen. The adsorption energy, 2.15 eV, shown in Table 1, was calculated by assuming that each H atom comes from a dissociated acetic acid molecule (i.e., $2CH_3COOH \rightarrow 2CH_3COO + H_2$). To facilitate the comparison with the other adsorption energies, the resulting value is reported in electronvolts per acetic acid molecule. If, however, we assume that a H atom is freely available (i.e., $CH_3COOH + H \rightarrow CH_3COO + H_2$), the adsorption energy increases to 4.79 eV. On a clean surface, a hydrogen atom can be first adsorbed on the substrate. In this case, in order for the formation of a H_2 molecule to take place, the energy gained from the formation of the H−H bond (4.52 eV[84]) and the adsorption of the resulting H_2 molecule has to outmatch the energy of the Fe−H bonds (2.60 eV[85]). Since the absorption of H_2 is weak (0.11 eV[85]) and two Fe−H bonds are involved, the formation of H_2 appears unlikely. This idea was further investigated by constructing a supercell with the acetate, as in Figure 3b, and two hydrogen atoms, one on the H2 position and a second one in the closest bridge site to it. During the relaxation of this system the distance between these two hydrogens increased until both atoms were adsorbed on hollow positions. Moreover, the total energy of this system is 0.55 eV lower than the energy of the acetate + H_2 system, indicating, once again, that in this case the adsorption of H on the metallic surface is favored over the formation of hydrogen gas. On the other hand, if a second hydrogen is available at a relatively low energy cost, for example, from a hydronium cation, the considerable adsorption energy mentioned above indicates that the formation of hydrogen gas is plausible.

Water Layer on Fe(100). For the adsorption of molecular water on an Fe(100) surface, the formation of a monolayer where the water molecules alternate orientations to form a "zigzag" pattern (Figure 4a) is energetically favorable. The water molecules are adsorbed on the top sites of the metallic surface (but slightly shifted toward the bridge site), in agreement with previous studies where the adsorption of a single water molecule was considered.[55,57,60,61] This suggests that the adsorption site preference is not modified by this high water coverage. This may be caused by the reasonably good match between the calculated lattice constant of bcc Fe (2.83 Å) and the average distance between oxygens in water (2.81 Å[86]). In this configuration there are two nonequivalent water molecules, one with both O−H bonds nearly parallel to the surface (from here on, referred to simply as parallel) and the other with one O−H bond pointing to the slab (referred to as upward). For the former, the distance between the oxygen and the closest iron atom is 2.28 Å and for the latter, 3.35 Å. Besides the orientation, the only additional difference between the upward and parallel water molecule is the bond angle. The parallel water molecule has a bond angle of 105.36°, and in the upward molecule, the bond angle is equal to 104.20°. To determine this structure, several configurations (Figure 4) were relaxed with diverse algorithms. In these configurations, the orientation of the water molecules and their respective adsorption sites were varied. In a different approach, a simulated annealing in a supercell containing four water molecules adsorbed in a (2 × 2) surface cell results in an almost "zigzag" configuration which is, nonetheless, higher in energy (+266 meV). The main differences in geometry are a higher distance between the slab and the upward water molecules (4.30 Å) as well as the tilting of one O−H in bond in a parallel water molecule toward the slab.

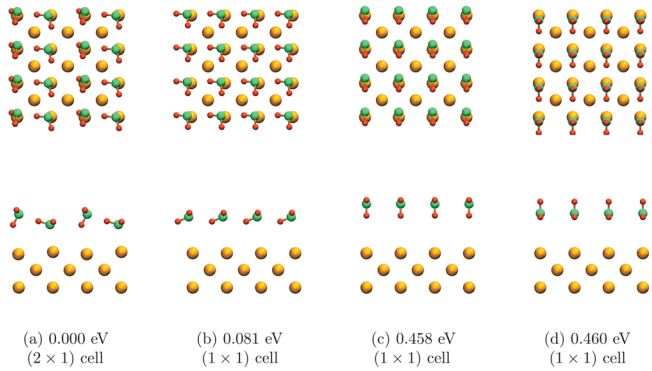

Figure 4. Some of the various configurations considered for the water layer and their difference in energy with respect to the lowest energy configuration. The various supercells employed for the simulations are here replicated along the axes parallel to the surface to facilitate their comparison.

In the proposed equilibrium water layer (Figure 4a), the average adsorption energy of each water molecule is 0.51 eV. The average adsorption energy per molecule was calculated according to the following equation

$$E_{ads} = \frac{1}{2}(E_{tot}^{H_2O+Fe(100)} - 2E_{tot}^{H_2O} - E_{tot}^{Fe(100)}) \quad (4)$$

where $E_{tot}^{H_2O+Fe(100)}$ is the total energy of the water molecules adsorbed on the Fe(100) slab, $E_{tot}^{Fe(100)}$ is the total energy of the clean Fe(100) surface, and $E_{tot}^{H_2O}$ is the total energy of the isolated water molecule. The difference between the average adsorption energy per water molecule of this layer and the one calculated for the single water molecule with GGA (0.39 eV[57]) can be attributed to the lateral intermolecular interactions and to the fact that dispersion forces are included in our calculation.

Isooctane, Ethanol, and Acetic Acid on a Water-Covered Fe(100) Surface. A water layer does not significantly change the adsorption geometry of isooctane.

dx.doi.org/10.1021/jp504695m | J. Phys. Chem. C 2014, 118, 21428−21437

The previously found equilibrium geometry of isooctane (Figure 1b) was placed on top of the Fe(100) + zigzag water system (Figure 4a). Because of the alternating orientation of the water molecules in the zigzag layer, there exists two possible top adsorption sites, one covered with a parallel water molecule and the other with an upward water molecule. The difference in unrelaxed adsorption energies (75 meV) between these sites shows no significant preference for one site over the other. Nevertheless, the equilibrium geometry of isooctane adsorbed on a water-covered Fe(100) surface was obtained by positioning the longest continuous carbon chain of the molecule along the slightly more stable site, which in this case is the one covered with a parallel water molecule, and relaxing the system afterward. The resulting equilibrium structure (Figure 5)

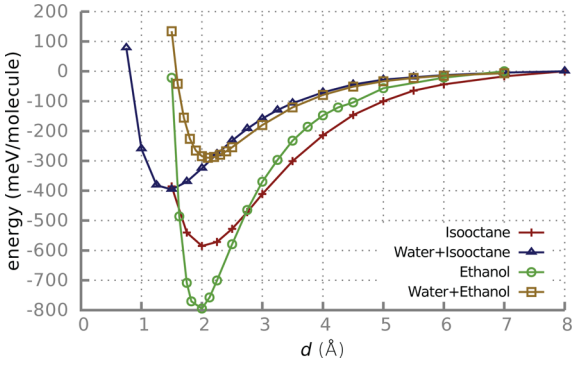

Figure 5. Calculated adsorption energy of the isooctane and ethanol molecules adsorbed on an Fe(100) surface (with and without a water layer) as a function of the vertical distance.

exhibits small geometrical changes in the isooctane molecule. The variation of bond lengths are on the order of 10^{-3} Å, and in angles the largest changes are of the order of 10^{-1} deg. There is, however, a more notable displacement of the water layer and the first layer of the slab away from the molecule (≈ 0.15 and ≈0.10 Å, respectively).

A water layer reduces the adsorption energy of isooctane on Fe(100) by 0.19 eV (Table 1). In the absence of a water layer, the isooctane molecule induces a nonisotropic accumulation of charge between the slab and the molecule and a deficit of charge in the region surrounding the molecule (Figure 7a). The

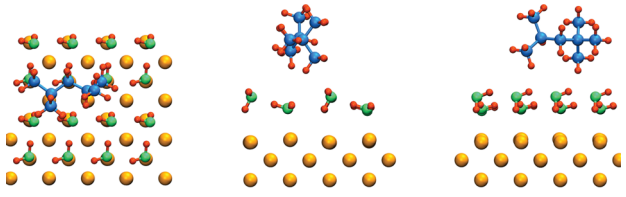
(a) Top view (b) Side view (c) Side view

Figure 6. Equilibrium structure of isooctane adsorbed on a water-covered Fe(100) surface.

forces arising from this redistribution of charge lead to binding. With the introduction of a water layer, the charge redistribution in the slab caused by the proximity of the isooctane molecule is considerably reduced (Figure 7b). The water molecules "screen" the interaction between them, and consequently, the region surrounding the molecule also presents a lesser charge deficit, leading to weaker binding. The lesser charge redistribution in the water layer combined with its screening

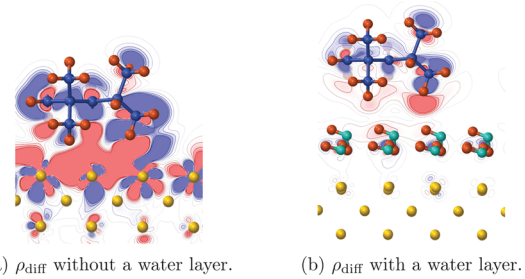
(a) ρ_{diff} without a water layer. (b) ρ_{diff} with a water layer.

Figure 7. Comparison of the charge density difference (ρ_{diff}) of isooctane adsorbed on the bcc Fe(100) surface at the equilibrium distance with and without a water layer. In the absence of a water layer, the charge density difference is defined as $\rho_{diff} = \rho - (\rho_{isooctane} + \rho_{Fe(100)})$, where ρ denotes the charge density of the isooctane adsorbed on Fe(100), while $\rho_{isooctane}$ and $\rho_{Fe(100)}$ represent the charge densities of the isolated molecule and clean Fe(100) slab, respectively. In the presence of a water layer, the definition changes to $\rho_{diff} = \rho - (\rho_{isooctane} + \rho_{Fe(100)+WL})$, where $\rho_{Fe(100)+WL}$ is the charge density of the water-covered Fe(100) slab. The charge difference is plotted in a plane perpendicular to the surface for values between -5×10^{-4} electrons/Å^3 (solid blue, deficit) and 5×10^{-4} electrons/Å^3 (solid red, accumulation).

effects allows the isooctane molecule to form a shorter bond to the water layer than to the clean iron surface (Figure 6).

The presence of a water layer favors a different adsorption configuration of the ethanol molecule (Figure 8). Since a

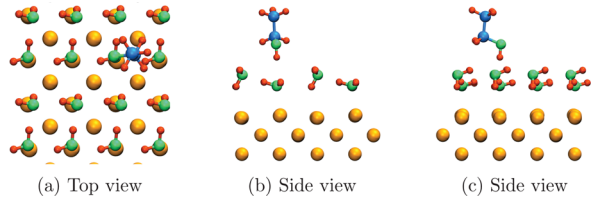
(a) Top view (b) Side view (c) Side view

Figure 8. Equilibrium structure of ethanol adsorbed on a water-covered Fe(100) surface.

relatively strong interaction between the hydroxyl group of the ethanol and the water layer is expected, an adsorption analysis was carried out taking configurations 1–3 (Figure 2a–c) into account. The ethanol molecule of each configuration was placed above a water-covered Fe(100) surface and subsequently relaxed (Figure 9). In all cases the top adsorption site covered with a parallel water molecule was preferred. In the presence of water, the adsorption energy of configuration 2 is approximately 5 meV larger than the corresponding one for configuration 3, which is one of the equilibrium configurations in the absence of water. The stabilization of this structure is likely caused by the hydrogen bond between the oxygen of the water molecules and the hydroxyl group of ethanol. The small energy difference suggests, nevertheless, that no particular orientation is favored at room temperature.

The adsorption energy of ethanol on Fe(100) decreases by 0.51 eV in the presence of a water layer (Table 1). This decrease is considerable higher than the one occurring in the isooctane case. A previous study[12] showed that ethanol binds to the Fe(100) surface via dispersion forces and a weak electrostatic interaction between the oxygen of the hydroxyl group and the Fe(100) surface. These interactions, together with the Pauli repulsion, lead to a charge redistribution, where the electron density in a region surrounding the hydroxyl

dx.doi.org/10.1021/jp504695m | J. Phys. Chem. C 2014, 118, 21428–21437

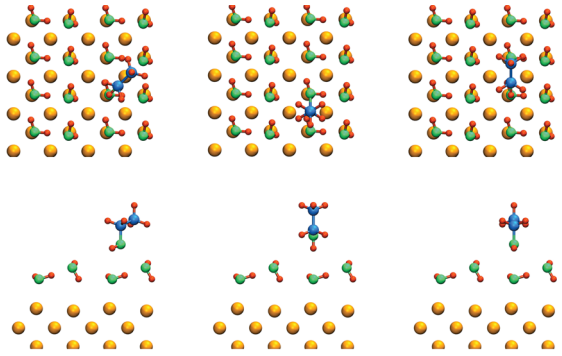

(a) Config. 1 (b) Config. 2 (c) Config. 3

Figure 9. Configurations considered for the adsorption of an ethanol molecule on a water-covered Fe(100) surface, here displayed with the molecule on the top adsorption site at a distance d = 2.00 Å. The top row displays the top view of the system, while the bottom row is the side view.

changes (Figure 10a). With the introduction of a water layer, the size of this region decreases significantly (Figure 10b).

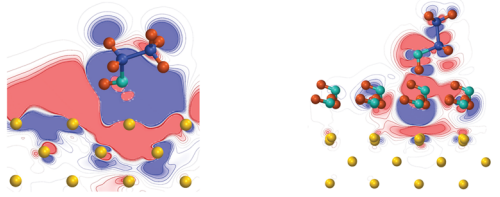

(a) ρ_{diff} without a water layer. (b) ρ_{diff} with a water layer.

Figure 10. Comparison of the charge density difference (ρ_{diff}) of ethanol adsorbed on the bcc Fe(100) surface at the equilibrium distance with and without a water layer. The charge density difference is defined and plotted analogously to Figure 7.

Furthermore, since the redistribution of charge in the top layer of the slab was mainly caused the hydroxyl group of the ethanol molecule, the water layer screens its effect more efficiently. As a consequence, only the iron atom directly below the hydroxyl group "feels" the interaction. The combination of these effects results in a weaker bond.

With the introduction of a water layer, the adsorption configuration of the acetate molecule is moderately changed (Figure 11). As a first approximation to determine the preferred

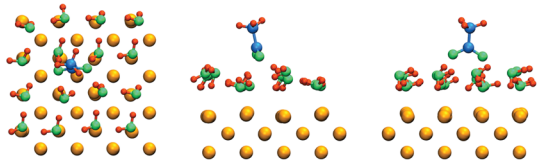

(a) Top view (b) Side view (c) Side view

Figure 11. Equilibrium structure of acetate adsorbed on a water-covered Fe(100) surface.

adsorption site, the binding energies of two different sites were calculated. The energy of acetate adsorbed on the top site covered with a parallel water molecule is ≈0.21 eV lower than the one covered with an upward water molecule. Relaxing the more stable structure produced notable changes in both the acetate molecule and the water layer. The acetate molecule is displaced toward the bridge position, the O−C−O angle is reduced by 0.17°, and the C−C bond is tilted by 12.13° with respect to the surface normal. On the water layer, the four water molecules closest to the acetate reorient their O−H bonds to "point" toward the closest oxygen of the acetate molecule. This can be attributed not only to the tendency of hydroxyl and oxygen to form hydrogen bonds but also to the higher chemical reactivity of the acetate caused by the odd number of valence electrons.

A water layer covering an Fe(100) surface increases the adsorption energy of the acetate molecule by 0.69 eV (Table 1). Without the water layer, the region surrounding the oxygen atoms of the acetate molecule accumulates a significant amount of charge (Figure 12a) while decreasing the charge in the

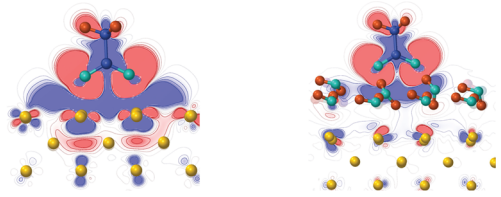

(a) ρ_{diff} without a water layer. (b) ρ_{diff} with a water layer.

Figure 12. Comparison of the charge density difference (ρ_{diff}) of acetate adsorbed on the bcc Fe(100) surface at the equilibrium distance with and without a water layer. The charge density difference is defined and plotted analogously to Figure 7 but with the charge density difference between values of -5×10^{-3} and 5×10^{-3} electrons/Å^3, which are 1 order of magnitude larger than the plotted ρ_{diff} of isooctane and ethanol.

region above the slab. The attractive forces produced by the formation of regions of accumulation and deficit of charge are responsible for the binding between the acetate and the Fe(100) surface. The binding mechanism remains essentially the same after introducing the water layer, with the only difference being that the region where the charge is decreased now lies on the water molecules below the acetate molecule (Figure 12b). Moreover, the introduction of a water layer allows the formation of hydrogen bonds between the oxygen atoms of the acetate and the hydroxyl group of the water molecules, which may account for the increase in the adsorption energy and decrease in the equilibrium distance (Figure 14).

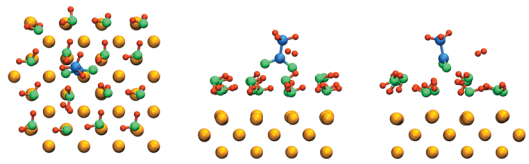

(a) Top view (b) Side view (c) Side view

Figure 13. Equilibrium structure of the dissociated acetic acid adsorbed on a water-covered Fe(100) surface.

The presence of a water layer increases the binding energy of the dissociated acetic acid and promotes the formation of hydrogen gas. To study the acetic acid, a hydrogen atom was introduced in the acetate−water−Fe(100) system described above and placed on top of an upward water molecule on the position analogous to H1 in the water-free system (Figure 3b). During the relaxation of this system, the dissociated hydrogen and a hydrogen of its closest parallel water molecule (in direction away from the acetate) react to produce hydrogen gas.

dx.doi.org/10.1021/jp504695m | J. Phys. Chem. C 2014, 118, 21428−21437

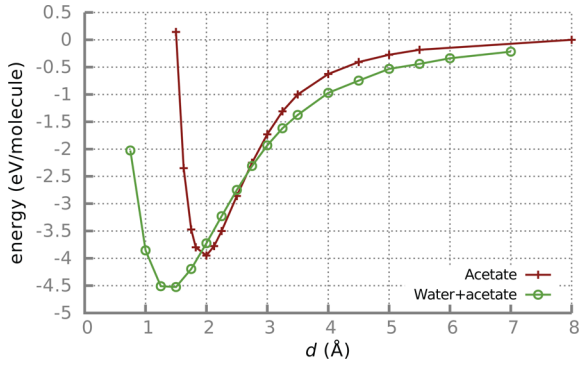

Figure 14. Calculated adsorption energy of acetate adsorbed on an Fe(100) surface (with and without a water layer) as a function of the vertical distance.

This process reduces the energy of the system by ≈2 eV. This considerable amount of energy and the fact that this equilibrium state was reached through an ionic relaxation indicate that other reaction paths for the dissociated hydrogen are questionable. The resulting adsorption energy is 0.70 eV larger than the corresponding system without the water layer (Table 1), where the dissociated hydrogen is adsorbed on the metallic surface. The water molecules of the layer help to stabilize the resulting acetate and hydroxyl group by reorienting themselves to facilitate the formation of hydrogen bonds with them (Figure 13).

CONCLUSION

The effect of a water layer on the adsorption of organic molecules on an Fe(100) surface strongly depends on the type of bond between them. In those molecules, where dispersion forces contribute significantly to the binding mechanism, the water layer has a stronger screening effect. Additionally, this effect can be enhanced by the presence of polar functional groups in the molecule. The type of functional group plays also an important role in defining the geometry of the equilibrium configurations; if they contribute to the formation of hydrogen bonds, a different adsorption geometry may be stabilized through them, as in the case of ethanol, and an increase in the adsorption energy can take place like for acetic acid. With the introduction of a water layer, there is a moderate reduction of the adsorption energy of isooctane on Fe(100) but no significant change in the equilibrium geometries. In comparison, ethanol exhibits a larger decrease of the adsorption energy and a change in the adsorption configuration. On the other hand, the adsorption energy of acetic acid is increased and there is a moderate change in the equilibrium geometry. We expect that our results can be extrapolated to a wider amount of substances. For instance, as long as the same corresponding binding mechanism takes place, alkanes, alcohols with short carbon chains, and (short chain) carboxylic acids may exhibit similar effects in the adsorption energies and equilibrium geometries with the introduction of a water layer as isooctane, ethanol, and acetic acid, respectively.

The increase in production and use of fuels containing biocomponents has triggered a considerable amount of research focused on improving their combustion efficiency. As our results demonstrate, it is also important to consider how these substances interact with surfaces and how they affect such interactions of components already present in conventional fuels. In particular, we showed that the presence of water may have an undesirable (or desirable) impact for substances whose usefulness is directly related to their adsorption properties, as in the case of lubricity additives. We anticipate that the potential energy curves produced will aid in the fitting of accurate surface−lubricant interaction potentials used by other methods, such as classical molecular dynamics simulations, where the influence of additional variables can be analyzed to improve our description and understanding of these lubricated systems.

ASSOCIATED CONTENT

Supporting Information

Adsorption energies of the various configurations of isooctane, ethanol, acetate, and acetic acid adsorbed on an Fe(100) surface as a function of the vertical distance. This material is available free of charge via the Internet at http://pubs.acs.org/.

AUTHOR INFORMATION

Corresponding Author

*E-mail: pb@cms.tuwien.ac.at.

Notes

The authors declare no competing financial interest.

ACKNOWLEDGMENTS

P.O.B., G.F., J.R., and P.M. acknowledge support from the Austrian Science Funds (FWF) within the SFB ViCoM F4109-N13 P09. Part of this work was funded by the Austrian COMET Program (Project K2 XTribology, Grant No. 824187) and was carried out at the "Excellence Centre of Tribology" (AC2T research GmbH). The computational results presented have been achieved in part using the Vienna Scientific Cluster (VSC).

REFERENCES

(1) IEA. *Tracking Clean Energy Progress 2013*; International Energy Agency: Paris, 2013.

(2) Breen, J. P.; Burch, R.; Coleman, H. M. Metal-Catalysed Steam Reforming of Ethanol in the Production of Hydrogen for Fuel Cell Applications. *Appl. Catal., B* **2002**, *39*, 65−74.

(3) Liguras, D. I.; Kondarides, D. I.; Verykios, X. E. Production of Hydrogen for Fuel Cells by Steam Reforming of Ethanol Over Supported Noble Metal Catalysts. *Appl. Catal., B* **2003**, *43*, 345−354.

(4) Deluga, G. A.; Salge, J. R.; Schmidt, L. D.; Verykios, X. E. Renewable Hydrogen from Ethanol by Autothermal Reforming. *Science* **2004**, *303*, 993−997.

(5) Frusteri, F.; Freni, S.; Spadaro, L.; Chiodo, V.; Bonura, G.; Donato, S.; Cavallaro, S. H_2 Production for MC Fuel Cell by Steam Reforming of Ethanol over MgO Supported Pd, Rh, Ni and Co Catalysts. *Catal. Commun.* **2004**, *5*, 611−615.

(6) Takahashi, H.; Hisaoka, S.; Nitta, T. Ethanol Oxidation Reactions Catalyzed by Water Molecules: $CH_3CH_2OH+nH_2O \rightarrow CH_3CHO+H_2+nH_2O$ (n=0,1,2). *Chem. Phys. Lett.* **2002**, *363*, 80−86.

(7) Haryanto, A.; Fernando, S.; Murali, N.; Adhikari, S. Current Status of Hydrogen Production Techniques by Steam Reforming of Ethanol: A Review. *Energy Fuels* **2005**, *19*, 2098−2106.

(8) Duan, S.; Senkan, S. Catalytic Conversion of Ethanol to Hydrogen Using Combinatorial Methods. *Ind. Eng. Chem. Res.* **2005**, *44*, 6381−6386.

(9) Kowal, A.; Li, M.; Shao, M.; Sasaki, K.; Vukmirovic, M.; Zhang, J. h.; Marinkovic, N.; Liu, P.; Frenkel, A.; Adzic, R. Ternary Pt/Rh/SnO_2 Electrocatalysts for Oxidizing Ethanol to CO_2. *Nat. Mater.* **2009**, *8*, 325−330.

(10) Ni, M.; Leung, D. Y. C.; Leung, M. K. H. A Review on Reforming Bio-Ethanol for Hydrogen Production. *Int. J. Hydrogen Energy* **2007**, *32*, 3238−3247 (International Symposium on Solar-Hydrogen-Fuel Cells 2005).

(11) Kohn, W.; Sham, L. J. Self-Consistent Equations Including Exchange and Correlation Effects. *Phys. Rev.* **1965**, *140*, A1133−A1138.
(12) Bedolla, P.; Feldbauer, G.; Wolloch, M.; Eder, S. J.; Dörr, N.; Mohn, P.; Redinger, J.; Vernes, A. Effects of van der Waals Interactions in the Adsorption of Isooctane and Ethanol on Fe(100) Surfaces. *J. Phys. Chem. C* **2014**, *118*, 17608−17615.
(13) Dion, M.; Rydberg, H.; Schröder, E.; Langreth, D. C.; Lundqvist, B. I. van der Waals Density Functional for General Geometries. *Phys. Rev. Lett.* **2004**, *92*, 246401.
(14) Lee, K.; Murray, E. D.; Kong, L.; Lundqvist, B. I.; Langreth, D. C. Higher-Accuracy van der Waals Density Functional. *Phys. Rev. B* **2010**, *82*, 081101.
(15) Sato, T.; Tsuneda, T.; Hirao, K. Long-Range Corrected Density Functional Study on Weakly Bound Systems: Balanced Descriptions of Various Types of Molecular Interactions. *J. Chem. Phys.* **2007**, *126*.
(16) Sato, T.; Nakai, H. Density Functional Method Including Weak Interactions: Dispersion Coefficients Based on the Local Response Approximation. *J. Chem. Phys.* **2009**, *131*, 224104.
(17) Sato, T.; Nakai, H. Local Response Dispersion Method. II. Generalized Multicenter Interactions. *J. Chem. Phys.* **2010**, *133*, 194101.
(18) Grimme, S. Semiempirical GGA-type Density Functional Constructed with a Long-Range Dispersion Correction. *J. Comput. Chem.* **2006**, *27*, 1787−1799.
(19) Grimme, S.; Antony, J.; Ehrlich, S.; Krieg, H. A Consistent and Accurate Ab Initio Parametrization of Density Functional Dispersion Correction (DFT-D) for the 94 Elements H−Pu. *J. Chem. Phys.* **2010**, *132*.
(20) Grimme, S. Density Functional Theory with London Dispersion Corrections. *Comput. Mol. Sci.* **2011**, *1*, 211−228.
(21) Antony, J.; Grimme, S. Density Functional Theory Including Dispersion Corrections for Intermolecular Interactions in a Large Benchmark Set of Biologically Relevant Molecules. *Phys. Chem. Chem. Phys.* **2006**, *8*, 5287−5293.
(22) von Lilienfeld, O. A.; Tavernelli, I.; Rothlisberger, U.; Sebastiani, D. Optimization of Effective Atom Centered Potentials for London Dispersion Forces in Density Functional Theory. *Phys. Rev. Lett.* **2004**, *93*, 153004.
(23) von Lilienfeld, A. O.; Tkatchenko, A. Two- and Three-Body Interatomic Dispersion Energy Contributions to Binding in Molecules and Solids. *J. Chem. Phys.* **2010**, *132*, 234109.
(24) Becke, A. D.; Johnson, E. R. Exchange-Hole Dipole Moment and the Dispersion Interaction Revisited. *J. Chem. Phys.* **2007**, *127*.
(25) Tkatchenko, A.; Scheffler, M. Accurate Molecular van der Waals Interactions from Ground-State Electron Density and Free-Atom Reference Data. *Phys. Rev. Lett.* **2009**, *102*, 073005.
(26) Tkatchenko, A.; Romaner, L.; Hofmann, O. T.; Zojer, E.; Ambrosch-Draxl, C.; Scheffler, M. van der Waals Interactions Between Organic Adsorbates and at Organic/Inorganic Interfaces. *MRS Bull.* **2010**, *35*, 435−442.
(27) Tkatchenko, A.; DiStasio, R. A.; Car, R.; Scheffler, M. Accurate and Efficient Method for Many-Body van der Waals Interactions. *Phys. Rev. Lett.* **2012**, *108*, 236402.
(28) Cole, M. W.; Velegol, D.; Kim, H.-Y.; Lucas, A. A. Nanoscale van der Waals Interactions. *Macromol. Symp.* **2009**, *35*, 849−866.
(29) Dobson, J. F.; Dinte, B. P. Constraint Satisfaction in Local and Gradient Susceptibility Approximations: Application to a van der Waals Density Functional. *Phys. Rev. Lett.* **1996**, *76*, 1780−1783.
(30) Furche, F. Molecular Tests of the Random Phase Approximation to the Exchange−Correlation Energy Functional. *Phys. Rev. B* **2001**, *64*, 195120.
(31) Furche, F.; Van Voorhis, T. Fluctuation−Dissipation Theorem Density-Functional Theory. *J. Chem. Phys.* **2005**, *122*, 164106.
(32) Ángyán, J. G.; Liu, R.-F.; Toulouse, J.; Jansen, G. Correlation Energy Expressions from the Adiabatic-Connection Fluctuation−Dissipation Theorem Approach. *J. Chem. Theory Comput.* **2011**, *7*, 3116−3130.
(33) Heßelmann, A. Random-Phase-Approximation Correlation Method Including Exchange Interactions. *Phys. Rev. A* **2012**, *85*, 012517.
(34) Harl, J.; Kresse, G. Accurate Bulk Properties from Approximate Many-Body Techniques. *Phys. Rev. Lett.* **2009**, *103*, 056401.
(35) Riley, K. E.; Pitoňák, M.; Jurečka, P.; Hobza, P. Stabilization and Structure Calculations for Noncovalent Interactions in Extended Molecular Systems Based on Wave Function and Density Functional Theories. *Chem. Rev.* **2010**, *110*, 5023−5063.
(36) Kannemann, F. O.; Becke, A. D. van der Waals Interactions in Density-Functional Theory: Intermolecular Complexes. *J. Chem. Theory Comput.* **2010**, *6*, 1081−1088.
(37) Steinmann, S. N.; Corminboeuf, C. Comprehensive Benchmarking of a Density-Dependent Dispersion Correction. *J. Chem. Theory Comput.* **2011**, *7*, 3567−3577.
(38) Misquitta, A. J.; Podeszwa, R.; Jeziorski, B.; Szalewicz, K. Intermolecular Potentials Based on Symmetry-Adapted Perturbation Theory with Dispersion Energies from Time-Dependent Density-Functional Calculations. *J. Chem. Phys.* **2005**, *123*, 075312.
(39) Johnson, E. R.; Becke, A. D. A Post-Hartree−Fock Model of Intermolecular Interactions. *J. Chem. Phys.* **2005**, *123*, 024101.
(40) Silvestrelli, P. L. van der Waals Interactions in DFT Made Easy by Wannier Functions. *Phys. Rev. Lett.* **2008**, *100*, 053002.
(41) Vydrov, O. A.; Van Voorhis, T. Nonlocal van der Waals Density Functional: The Simpler the Better. *J. Chem. Phys.* **2010**, *133*, 244103.
(42) Cooper, V. R.; Kong, L.; Langreth, D. C. Computing Dispersion Interactions in Density Functional Theory. *Phys. Procedia* **2010**, *3*, 1417−1430 [Proceedings of the 22th Workshop on Computer Simulation Studies in Condensed Matter Physics (CSP 2009)].
(43) Graziano, G.; Klimeš, J.; Fernandez-Alonso, F.; Michaelides, A. Improved Description of Soft Layered Materials with van der Waals Density Functional Theory. *J. Phys.: Condens. Matter* **2012**, *24*, 424216.
(44) Chakarova-Käck, S. D.; Schröder, E.; Lundqvist, B. I.; Langreth, D. C. Application of van der Waals Density Functional to an Extended System: Adsorption of Benzene and Naphthalene on Graphite. *Phys. Rev. Lett.* **2006**, *96*, 146107.
(45) Mittendorfer, F.; Garhofer, A.; Redinger, J.; Klimeš, J.; Harl, J.; Kresse, G. Graphene on Ni(111): Strong Interaction and Weak Adsorption. *Phys. Rev. B* **2011**, *84*, 201401.
(46) Vanin, M.; Mortensen, J. J.; Kelkkanen, A. K.; Garcia-Lastra, J. M.; Thygesen, K. S.; Jacobsen, K. W. Graphene on Metals: A van der Waals Density Functional Study. *Phys. Rev. B* **2010**, *81*, 081408.
(47) Chen, D.-L.; Al-Saidi, W. A.; Johnson, J. K. Noble Gases on Metal Surfaces: Insights on Adsorption Site Preference. *Phys. Rev. B* **2011**, *84*, 241405.
(48) Sony, P.; Puschnig, P.; Nabok, D.; Ambrosch-Draxl, C. Importance of van der Waals Interaction for Organic Molecule−Metal Junctions: Adsorption of Thiophene on Cu(110) as a Prototype. *Phys. Rev. Lett.* **2007**, *99*, 176401.
(49) Liu, W.; Carrasco, J.; Santra, B.; Michaelides, A.; Scheffler, M.; Tkatchenko, A. Benzene Adsorbed on Metals: Concerted Effect of Covalency and van der Waals bonding. *Phys. Rev. B* **2012**, *86*, 245405.
(50) Li, G.; Tamblyn, I.; Cooper, V. R.; Gao, H.-J.; Neaton, J. B. Molecular Adsorption on Metal Surfaces with van der Waals Density Functionals. *Phys. Rev. B* **2012**, *85*, 121409.
(51) Lee, K.; Morikawa, Y.; Langreth, D. C. Adsorption of *n*-Butane on Cu(100), Cu(111), Au(111), and Pt(111): van der Waals Density-Functional Study. *Phys. Rev. B* **2010**, *82*, 155461.
(52) Tereshchuk, P.; Da Silva, J. L. F. Ethanol and Water Adsorption on Close-Packed 3d, 4d, and 5d Transition-Metal Surfaces: A Density Functional Theory Investigation with van der Waals Correction. *J. Phys. Chem. C* **2012**, *116*, 24695−24705.
(53) Błoński, P.; López, N. On the Adsorption of Formaldehyde and Methanol on a Water-Covered Pt(111): A DFT-D Study. *J. Phys. Chem. C* **2012**, *116*, 15484−15492.
(54) Tereshchuk, P.; Da Silva, J. L. F. Density Functional Investigation of the Adsorption of Ethanol−Water Mixture on the Pt(111) Surface. *J. Phys. Chem. C* **2013**, *117*, 16942−16952.

(55) Freitas, R. R. Q.; Rivelino, R.; de Brito Mota, F.; de Castilho, C. M. C. Dissociative Adsorption and Aggregation of Water on the Fe(100) Surface: A DFT Study. *J. Phys. Chem. C* **2012**, *116*, 20306−20314.
(56) Eder, M.; Terakura, K.; Hafner, J. Initial Stages of Oxidation of (100) and (110) Surfaces of Iron Caused by Water. *Phys. Rev. B* **2001**, *64*, 115426.
(57) Jung, S. C.; Kang, M. H. Adsorption of a Water Molecule on Fe(100): Density-Functional Calculations. *Phys. Rev. B* **2010**, *81*, 115460.
(58) Karlický, F.; Lazar, P.; Dubecký, M.; Otyepka, M. Random Phase Approximation in Surface Chemistry: Water Splitting on Iron. *J. Chem. Theory Comput.* **2013**, *9*, 3670−3676.
(59) Dwyer, D. J.; Kelemen, S. R.; Kaldor, A. The Water Dissociation Reaction on Clean and Oxidized Iron (110). *J. Chem. Phys.* **1982**, *76*, 1832−1837.
(60) Lazar, P.; Otyepka, M. Dissociation of Water at Iron Surfaces: Generalized Gradient Functional and Range-Separated Hybrid Functional Study. *J. Phys. Chem. C* **2012**, *116*, 25470−25477.
(61) Govender, A.; Curulla Ferré, D.; Niemantsverdriet, J. The Surface Chemistry of Water on Fe(100): A Density Functional Theory Study. *ChemPhysChem* **2012**, *13*, 1583−1590.
(62) Klimeš, J.; Bowler, D. R.; Michaelides, A. van der Waals Density Functionals Applied to Solids. *Phys. Rev. B* **2011**, *83*, 195131.
(63) Kresse, G.; Hafner, J. Ab Initio Molecular Dynamics for Liquid Metals. *Phys. Rev. B* **1993**, *47*, 558.
(64) Kresse, G.; Hafner, J. Norm-Conserving and Ultrasoft Pseudopotentials for First-Row and Transition-Elements. *J. Phys.: Condens. Matter* **1994**, *6*, 8245.
(65) Kresse, G.; Hafner, J. Ab Initio Molecular-Dynamics Simulation of the Liquid-Metal−Amorphous-Semiconductor Transition in Germanium. *Phys. Rev. B* **1994**, *49*, 14251.
(66) Kresse, G.; Furthmüller, J. Efficient Iterative Schemes for Ab Initio Total-Energy Calculations Using a Plane-Wave Basis Set. *Phys. Rev. B* **1996**, *54*, 11169.
(67) Kresse, G.; Furthmüller, J. Efficiency of Ab-Initio Total Energy Calculations for Metals and Semiconductors Using a Plane-Wave Basis Set. *Comput. Mater. Sci.* **1996**, *6*, 15.
(68) Kresse, G.; Joubert, D. From Ultrasoft Pseudopotentials to the Projector Augmented-Wave Method. *Phys. Rev. B* **1999**, *59*, 1758.
(69) Blöchl, P. E. Projector Augmented-Wave Method. *Phys. Rev. B* **1994**, *50*, 17953−17979.
(70) Becke, A. D. On the Large-Gradient Behavior of the Density Functional Exchange Energy. *J. Chem. Phys.* **1986**, *85*, 7184−7187.
(71) Klimeš, J.; Bowler, D. R.; Michaelides, A. Chemical Accuracy for the van der Waals Density Functional. *J. Phys.: Condens. Matter* **2010**, *22*, 022201.
(72) Perdew, J. P.; Burke, K.; Ernzerhof, M. Generalized Gradient Approximation Made Simple. *Phys. Rev. Lett.* **1996**, *77*, 3865−3868.
(73) Perdew, J. P.; Burke, K.; Ernzerhof, M. Erratum: Generalized Gradient Approximation Made Simple. *Phys. Rev. Lett.* **1997**, *78*, 1396.
(74) Wyckoff, R. *Crystal Structures*; Interscience Publishers: New York, 1971; Vol. *2*.
(75) Monkhorst, H. J.; Pack, J. D. Special Points for Brillouin-Zone Integrations. *Phys. Rev. B* **1976**, *13*, 5188−5192.
(76) Methfessel, M.; Paxton, A. T. High-Precision Sampling for Brillouin-Zone Integration in Metals. *Phys. Rev. B* **1989**, *40*, 3616−3621.
(77) Grinter, D.; Nicotra, M.; Thornton, G. Acetic Acid Adsorption on Anatase TiO_2(101). *J. Phys. Chem. C* **2012**, *116*, 11643−11651.
(78) Liao, L.-F.; Lien, C.-F.; Lin, J.-L. FTIR Study of Adsorption and Photoreactions of Acetic Acid on TiO_2. *Phys. Chem. Chem. Phys.* **2001**, *3*, 3831−3837.
(79) Xu, C.; Koel, B. Adsorption and Reaction of CH_3COOH and CD_3COOD on the MgO(100) Surface: A Fourier Transform Infrared and Temperature Programmed Desorption Study. *J. Chem. Phys.* **1995**, *102*, 8158−8166.
(80) Gao, Q.; Hemminger, J. A Vibrational Spectroscopy Study of CH_3COOH, CH_3COOD and $13CD_3COOH$(D) Adsorption on Pt(111). I. Surface Dimer Formation and Hydrogen Bonding. *Surf. Sci.* **1991**, *248*, 45−56.
(81) Kim, H. J.; Cho, J. Density-Functional Calculations of the Adsorption and Reaction of Acetic Acid on Ge(001). *J. Phys. Chem. C* **2008**, *112*, 6947−6952.
(82) Yanagisawa, S.; Tsuneda, T.; Hirao, K. Matsuzaki, Theoretical Investigation of Adsorption of Organic Molecules Onto Fe(110) Surface. *THEOCHEM* **2005**, *716*, 45−60.
(83) Heckel, W.; Elsner, B. A. M.; Schulz, C.; Müller, S. The Role of Hydrogen on the Adsorption Behavior of Carboxylic Acid on TiO_2 Surfaces. *J. Phys. Chem. C* **2014**, *118*, 10771−10779.
(84) Blanksby, S. J.; Ellison, G. B. Bond Dissociation Energies of Organic Molecules. *Acc. Chem. Res.* **2003**, *36*, 255−263.
(85) Sorescu, D. C. First Principles Calculations of the Adsorption and Diffusion of Hydrogen on Fe(100) Surface and in the Bulk. *Catal. Today* **2005**, *105*, 44−65.
(86) Bergmann, U.; Di Cicco, A.; Wernet, P.; Principi, E.; Glatzel, P.; Nilsson, A. Nearest-Neighbor Oxygen Distances in Liquid Water and Ice Observed by X-Ray Raman Based Extended X-ray Absorption Fine Structure. *J. Chem. Phys.* **2007**, *127*, 174504.